Adsorption Kinetics and Mechanical Properties of Ultrathin Polyelectrolyte Multilayers: Liquid-Supported versus Solid-Supported Films

ARTICLE *in* THE JOURNAL OF PHYSICAL CHEMISTRY B · JUNE 2009

Impact Factor: 3.3 · DOI: 10.1021/jp811178a · Source: PubMed

6 AUTHORS, INCLUDING:

Eduardo Guzmán
Complutense University of Madrid
44 PUBLICATIONS **642** CITATIONS
SEE PROFILE

Hernán Ritacco
Instituto de Fisica del Sur CONICET - UNS
36 PUBLICATIONS **667** CITATIONS
SEE PROFILE

Francisco Ortega
Complutense University of Madrid
137 PUBLICATIONS **2,452** CITATIONS
SEE PROFILE

Ramón G Rubio
Complutense University of Madrid
207 PUBLICATIONS **2,700** CITATIONS
SEE PROFILE

THE JOURNAL OF PHYSICAL CHEMISTRY B

Article

Adsorption Kinetics and Mechanical Properties of Ultrathin Polyelectrolyte Multilayers: Liquid-Supported versus Solid-Supported Films

Eduardo Guzma#n, Herna#n Ritacco, Francisco Ortega,
Tatiana Svitova, C. J. Radke, and Ramo#n G. Rubio

J. Phys. Chem. B, **2009**, 113 (20), 7128-7137• Publication Date (Web): 29 April 2009

Adsorption Kinetics and Mechanical Properties of Ultrathin Polyelectrolyte Multilayers: Liquid-Supported versus Solid-Supported Films

Eduardo Guzmán,[†] Hernán Ritacco,[†] Francisco Ortega,[†] Tatiana Svitova,[‡] C. J. Radke,[‡] and Ramón G. Rubio*[,†]

Departamento de Química Física I, Facultad de Química, Universidad Complutense, 28040 Madrid, Spain, and Department of Chemical Engineering, University of California, Berkeley, California, 94720

Received: December 18, 2008; Revised Manuscript Received: March 2, 2009

Multilayers of sodium salt of poly(4-styrene sulfonate) (PSS) and poly(diallyl dimethyl ammonium) chloride (PDADMAC) have been built layer by layer (LbL) both at the solid/aqueous interface (solid supported) and the air/aqueous interface (liquid supported). For the solid-supported multilayers, the adsorption kinetics and the complex shear modulus were measured using a dissipative quartz crystal microbalance and a null ellipsometer. A bubble tensiometer was used to measure the adsorption kinetics and the elasticity modulus of the liquid-supported multilayers. At the solid/aqueous interface, adsorption kinetics changes with the number of adsorbed layers. However, at the air/aqueous interface, PSS dynamics were the same for all adsorbed layers except the first. Conversely, the adsorption kinetics of PDADMAC at the air/water surface differed between those layers close to the interface and those far from it. Multilayers grow at the air/water interface by an intrinsic-charge-compensation process, whereas, for the same ionic strengths, solid-supported layers deposit by the extrinsic-charge-compensation process. No significant differences were found between the recoverable dilational storage modulus of the liquid-supported multilayers and the real part of the shear modulus of the solid-supported ones built at the same ionic strength. The values of the modulus are in the MPa range, which corresponds to gel-like films. This result is in agreement with the strong hydration degree of the LbL films calculated from ellipsometry measurements.

Introduction

Most devices of nanometer scale are subject to strong external stresses and perturbations. The mechanical properties of these devices must ensure their integrity under stress.[1] Thin polymer films are frequently used as coatings,[2] and more recently to build nanosized containers[3,4] for drug delivery.[5] Mechanical properties (e.g., the complex elasticity modulus) are important for acceptable performance of the thinnest polymer films (polymer monolayers) as emulsion and foam stabilizers.[6] During the last two decades, debate has focused on the possibility that the physical properties of nanoscale-confined polymers can be very different from those in bulk.[7] The glass-transition temperature, T_g, has been probably the most frequently studied property of thin polymer films.[8] Noticeable differences have been reported on how the film thickness affects T_g, depending on the strength of the interactions between the polymer chains and the solid surface.[9–12] In the present case of polymer films at the air/water and solid/water interfaces, the degree of hydration may strongly affect the mechanical properties of the film.[13]

Clearly, polymer films with thicknesses ranging from a few to a few hundred nanometers play important roles in systems characterized by length scales of the order of nanometers. Such films may be built on solid substrates or at fluid/fluid interfaces by a variety of methods.[14] In recent years, the layer-by-layer (LbL) or electrostatic self-assembly method has been developed and proven to be very versatile for building polyelectrolyte multilayers over a wide thickness range and at either solid substrates[15] or fluid/fluid interfaces.[16] At the same time, new methods have been developed for measuring the mechanical properties of both free-standing and solid-supported polymer films. In particular, Ferri et al. have described a simple method to measure the elasticity modulus for films formed at the surface of a liquid drop.[17] Also, Safouane et al. have applied an electrocapillary wave technique to determine the high frequency elasticity of a polyelectrolyte multilayer deposited on a flat air/liquid interface.[18] In the case of solid-supported films, atomic force microscopy (AFM) has been frequently used to determine the local mechanical properties of the polymer layers.[19,20] The dissipative quartz crystal microbalance (QCM) has also been shown to be a rather successful technique, since it can provide information about the mass adsorbed onto the quartz sensor, the kinetics of adsorption, and the mechanical properties of the adsorbed film (the complex shear modulus, G^*).[21] Moreover, the QCM technique can be easily adapted to the LbL procedure. Thus, all of the above information can be obtained as the multilayer grows, i.e., as a function of the thickness of the film.[22]

The purpose of this work is to build LbL films of a polyanion, sodium salt of poly(styrene sulfonate) (PSS), and a polycation, poly(diallyl dimethyl ammonium) chloride (PDADMAC), both at the air/water interface and at the solid/water interface. All films studied are, therefore, completely immersed in aqueous solution. The mechanism of multilayer growth for the PDADMAC/PSS combination has been described in detail in the literature.[23,24] The differences in adsorption kinetics of these polymers and the interfacial mechanical properties of their multilayers are the focus of this work.

* To whom correspondence should be addressed. E-mail: rgrubio@quim.ucm.es.
[†] Universidad Complutense.
[‡] University of California, Berkeley.

10.1021/jp811178a CCC: $40.75
Published on Web 04/29/2009

Experimental Section

The molecular weight of the sodium salt of poly(styrene sulfonate) was 70 kDa. The poly(diallyl dimethyl ammonium) chloride had a molecular weight in the 200−300 kDa range. NaCl was maintained at 200 °C under a vacuum for 1 week before use. Phosphate buffer (pH 7.0) was used in building the liquid-supported films at the air/water interface. All chemicals were purchased from Aldrich (Germany). The water was Milli-Q quality with a resistivity higher than 18 MΩ. Solutions were prepared by weight using an analytical balance with a precision of ±0.01 mg.

Solid/Water Interface. A dissipative quartz crystal microbalance (QCM) from KSV (model QCM Z-500, Finland) was used. Quartz crystals were AT-cut with one of the two gold electrodes in contact with the polymer solution. The characteristic frequency in a vacuum was $f_0 = 5$ MHz. A self-assembled monolayer of the sodium salt of 3-mercapto propanosulfonic acid [Na^+ $HS-(CH_2)_3-SO_3^-$] was initially built onto the gold electrode. The average surface charge was 10^{15} $-SO_3^-$ groups/cm^2 as calculated from the frequency shift in the adsorption experiment of thiol using the QCM. This result is in agreement with that of Love et al.[25] and also in agreement with the value obtained by a combination of potentiometric titration and ζ-potential measurements (Zeta Nanosizer, Malvern Instruments, U.S.) of a suspension of gold nanoparticles (diameter 13 ± 3 nm) on which a self-assembled monolayer (SAM) of the thiol was deposited (using the same protocol as followed for the quartz sensors) giving $\zeta = -39 \pm 5$ mV. QCM provided impedance spectra of the crystal for the fundamental mode and for odd overtones up to the 11th (central frequency $f_{11} = 55$ MHz).

We adopted the model of Johannsmann et al. to relate the change of the impedance spectra of the quartz sensor with the adsorbed mass and with the shear modulus of the adsorbed film.[26] Total adsorbed mass is given by

$$m^* = m^0\left[1 + \hat{J}(f)\frac{\rho_q(2\pi f)^2 h^2}{3}\right] \quad (1)$$

where

$$m^0 = -\frac{C\Delta f}{\nu} \quad (2)$$

and m^0 is the sensed mass obtained by the classical Sauerbrey equation, eq 2. Δf is the change in the frequency of the maximum of the impedance spectrum after contacting the sensor with the polymer solution ($\Delta f = f_0 - f$), ν is the overtone order (3, 5, 7, 9, and 11 in this work), and C is a constant characteristic of the quartz crystal properties ($C = 17.9$ ng·Hz^{-1}·cm^{-2} in this work). In eq 1, the real part of m^* is the true sensed mass after correcting m^0 for the viscoelastic character of the adsorbed layer. $\hat{J}(f)$ is the complex shear compliance, ρ_q is the density of quartz ($\rho_q = 19.3$ g·cm^{-3}), and h is the film thickness. Because different variables have to be determined from the impedance spectra (m^0 and $\hat{J}(f) = J' + iJ''$), it is necessary to measure the impedance spectra for several overtones. It is also necessary to provide a value for the viscosity of the polymer solution (measured with an oscillatory capillary rheometer in this work), as well as a value for the polymer density (in this work, we have used a density of 1.2 ± 0.1 g·cm^{-3}, which is a typical value used in polyelectrolyte multilayers[24]).

The null ellipsometer was from Nanofilm (Model EP3, Germany). To obtain the refractive index and thickness of the film, the ellipsometric angles Δ and Ψ were obtained as a function of the incident angle. These angles describe the changes in the state of polarization when the light is reflected at a surface.[27] Measured reflection may be described by the ratio of Fresnel reflection coefficients for the light-wave components parallel, r_p, and perpendicular, r_s, to the incidence plane[37] as related to the ellipsometric angles by

$$\frac{r_p}{r_s} = \tan\Psi e^{i\Delta} = \tan\Psi(\cos\Delta + i\sin\Delta) \quad (3)$$

Equilibrium values of Δ and Ψ were taken after successive readings and did not change for a 30 min period.

To obtain precise layer thicknesses, ellipsometric angles were measured using subphases of different refractive index obtained from mixtures of H_2O and D_2O.[21,28] The precision of Δ and Ψ was ±0.1 and ±0.05°, respectively. In order to calculate the adsorbed polymer mass, the refractive-index increment was measured[29] with a Brookhaven differential refractometer (Model BI-DNDC, U.S.). The precision in $(dn/dc)_T$ was ±0.001 (mL/g).

Air/Water Interface. The adsorption kinetics and step-relaxation experiments were performed using a sessile-bubble tensiometer previously described.[30] Aqueous-buffer rinsing (10 cell volumes) of each adsorbed polyelectrolyte layer and replacement of the aqueous subphase by a new polyelectrolyte solution was conducted following the flushing procedure described elsewhere.[30] The solution was stirred during rinsing and subphase replacement but was stopped during the adsorption kinetics measurements. Analysis of the volume and surface area of each bubble was done using an ADSA algorithm.[31] After equilibration of the surface tension, a fast step-expansion (less than 5% change in area) was carried out, and the shape and size of the bubble was monitored until a new equilibrium state was reached (change in surface tension was less than ±0.1 mN·m^{-1}).

For the ellipsometric experiments at the air/water surface, multilayers were built in a Langmuir trough (NIMA, model 102M, Coventry, U.K.). The rinsing procedure for aqueous-buffer flushing of the polymer film after each deposited layer and for substituting the subphase were the same as in the sessile-bubble experiments.

Results

Tensiometry. An air bubble (with a volume of 40 ± 5 μL) was formed in a phosphate buffered (pH 7.0) solution of PDADMAC (1 mg/mL) or PSS (1 mg/mL). The ionic strength of the solution was 0.15 M. PDADMAC was used for the first layer because PSS did not exhibit surface activity.[32] Only higher-molecular-weight PDADMAC (above approximately 100 kDa) adsorbs significantly at the air/water interface. Adsorption kinetics was followed by recording the air/water interfacial tension as a function of time with no stirring in the aqueous subphase. To evaluate the dynamic tension, the bubble profile was analyzed with the ADSA algorithm.[31] After completion of the tension dynamics of each layer, a step-expansion-relaxation of the bubble was performed and the film elasticity calculated. Finally, the adsorbed multilayer was rinsed with buffer solution. The entire process was then repeated by exposing the bubble to a buffered solution of the subsequent polyelectrolyte in the alternating LbL sequence. Throughout, PDADMAC layers are odd numbered and PSS are even numbered.

Figure 1 shows the time dependence of sequential PDADMAC/PSS polyelectrolyte tension dynamics in terms of surface pressure, $\gamma - \gamma_0$, for different numbers of adsorbed layers. Figure 1a shows the PDADMAC layers (odd), and

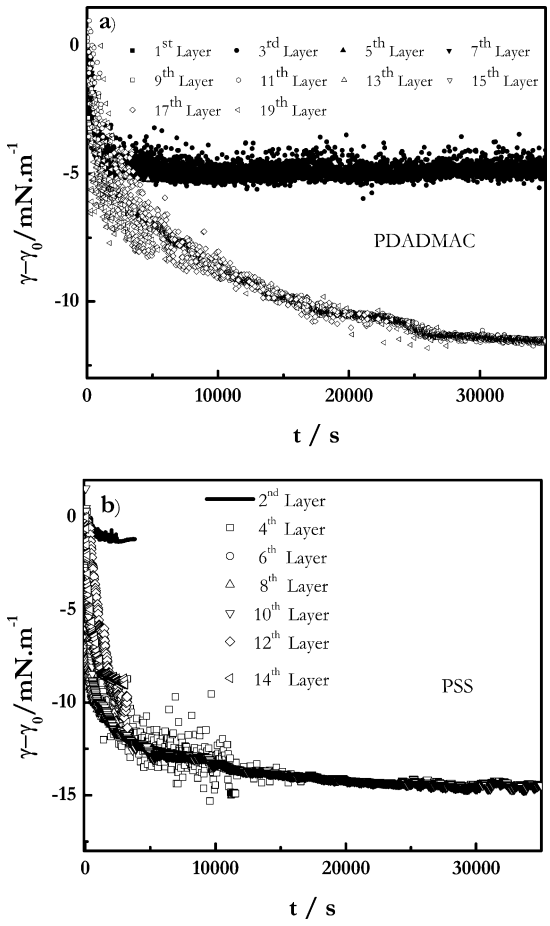

Figure 1. Tension dynamics of LbL polyelectrolyte layers at the aqueous solution/air interface where each curve corresponds to the adsorption process of an independent layer. γ is the surface tension of the film/air interface, and γ_0 is the surface tension of the film/air interface before each new adsorption step. (a) Kinetics of adsorption of PDADMAC layers (the first regime of the kinetics process is represented by solid symbols and the second regime by empty symbols). (b) Kinetics of adsorption of PSS layers (the kinetics of the first PSS layer is represented by a solid line and the other by empty symbols).

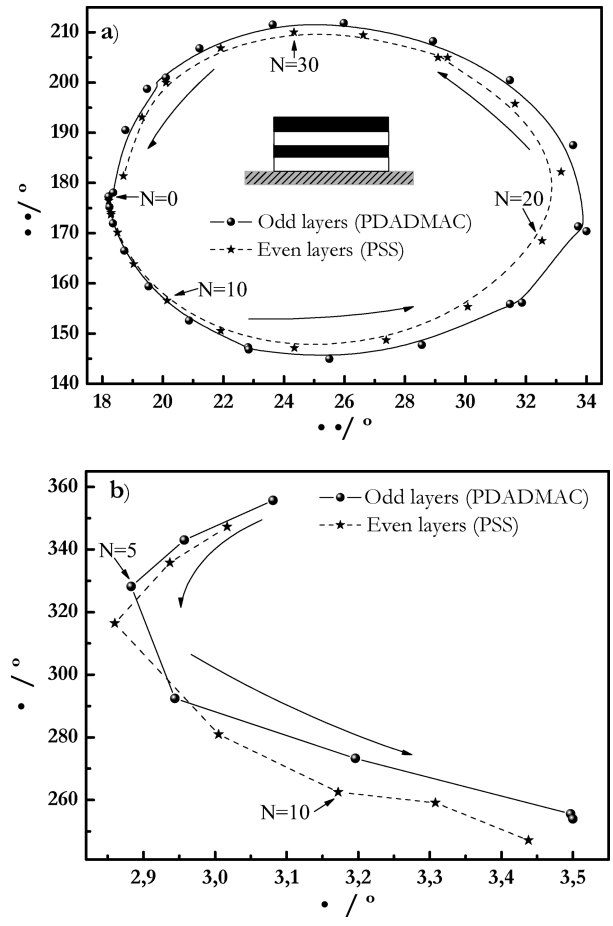

Figure 2. (a) Ellipsometric trajectory for the polyelectrolyte multilayer built at the solid/water interface at an ionic strength of [NaCl] = 300 mM. (b) Ellipsometric trajectory for the polyelectrolyte multilayer built at the aqueous solution/air interface for an ionic strength of I = 150 mM. N is the layer number, and the arrow specifies the direction of multilayer growth.

Figure 1b displays the PSS layers (even). γ_0 in these figures corresponds to the tension of the rinsed multilayer at the end of the previous layer addition. Many symbols overlap due to repeatability of the kinetic processes for the different layers. However, two well-differentiated adsorption kinetics were found for the PDADMAC layers (odd layers). Kinetic rates of PDADMAC polymer adsorption onto the PSS/water interface for films with less than seven layers were faster than those for thicker multilayered films. Except for the first layer of PSS (layer 2), the same dynamic−tension curve was obtained, regardless of the number of polymer layers built into the film.

Ellipsometry. Parts a and b of Figure 2 show the ellipsometric Δ-versus-Ψ trajectories obtained for the LbL multilayers built at the solid/water and air/water interfaces, respectively. Contrary to what one might expect for a completely homogeneous film,[33] there was a clearly pronounced odd−even effect in the ellipsometric angles for both interfaces. This effect may arise either from the changes in the refractive index or in the growth of the film thickness after each layer was added. Film optical thickness, h_{op}, of the LbL multilayers was then calculated from Δ−Ψ value sets measured at different angles and at different ratios of

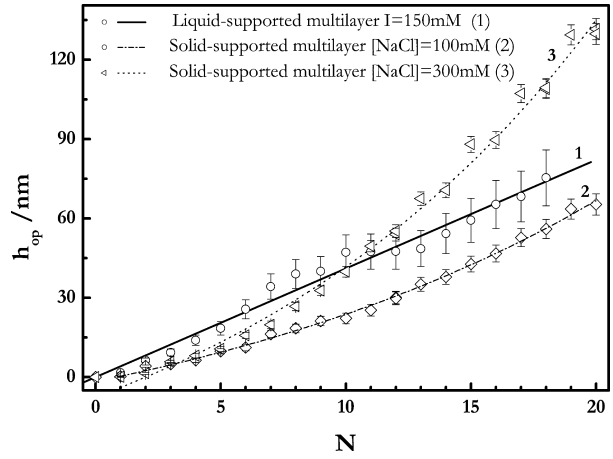

Figure 3. Optical thickness obtained from the ellipsometry measurements for (1) the multilayer built on an aqueous solution/air interface with a ionic strength of I = 150 mM and for (2, 3) multilayers built onto a solid surface at two different ionic strengths.

H_2O/D_2O in the subphase. Figure 3 reports h_{op} as a function of the layer number, N, both at the air/water (curve 1) and at the solid/water interfaces at different ionic strengths (curves 2 and 3). As in the previous cases, N = 1 corresponds to a first layer of PDADMAC.

The influence of aqueous-phase ionic strength on the LbL multilayer thickness has been studied for different multilayers

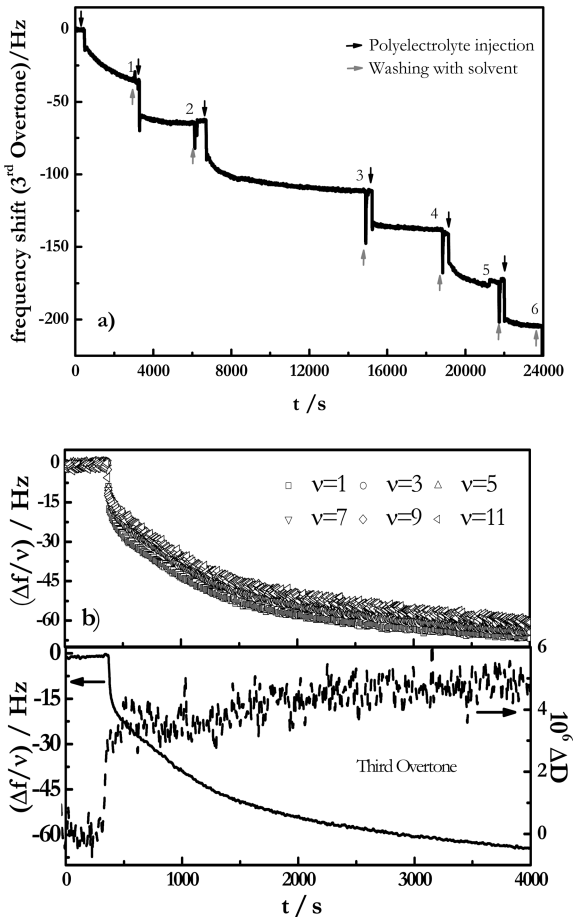

Figure 4. (a) Kinetics of the adsorption and washout processes for the first six layers of the PDADMAC+PSS films depicted as the time dependence of the shift of the central frequency of the third overtone of the quartz sensor. The experiments correspond to [NaCl] = 100 mM. (b) The upper panel shows the normalized frequency shift (shift of the central frequency, f, over the overtone order, ν, for $\nu = 1-11$. The lower panel shows the time dependence of $\Delta f(\nu = 3)$ and of the dissipation factor, D, for the adsorption of a layer of PDADMAC.

grown on solid surfaces;[24] it will also be discussed in detail in a future paper. In general, for an oppositely charged pair of strong polyelectrolytes and a given number of layers, the increase of the ionic strength in the aqueous solution leads to a thicker LbL multilayer. In Figure 3, differences in thickness growth became noticeable only for $N \geq 6$. In the case of the LbL multilayer grown at the air/water interface, the film thickness was slightly higher than that for those grown at the solid/water interface for a moderate number of layers ($N \leq 10$). For higher layer numbers, the air/water film thickness was closer to films built onto the solid surface from a solution with the same ionic strength. Consequently, after a few layers, the added polymer layer does not "feel" the original interface from which the multilayer was grown. These observations are in accord with the three-zone model of Decher.[15] For the air/water interface, Figure 3 shows that the film thickness increased linearly with N, whereas, for the solid/water interface with a concentration of NaCl in the aqueous phase ≥100 mM, film thickness grows faster than linearly (this growing regime is frequently referred to as the exponential regime, even though $h \sim \exp(N)$ may not strictly hold).

Dissipative Quartz Crystal Microbalance. Figure 4a shows the LbL building process for the first six layers (starting with PDADMAC) for [NaCl] = 100 mM in terms of the central frequency, f, of the third overtone of the D-QCM sensor. Similar results were found for other overtones. Adsorption dynamics were performed under static conditions without stirring as in the tensiometric and ellipsometric experiments. After adsorption of each layer, the D-QCM measurement chamber was cleaned with aqueous buffer to avoid bulk precipitation and then refilled with the desired polyelectrolyte solution. The filling process takes a few seconds and leads to the fast shifts of frequency seen in Figure 3 near washout events. These fast variations were not used in the analysis of the adsorption kinetics.

In addition to the expected decrease of f as a polymer mass adsorbed onto the quartz sensor, the washout process leads to a small shift of f. This is related to the reorganization of polymer chains in the film as a consequence of loss of some weakly bound polymer or swelling/deswelling. In any case, the change of frequency during washout was much smaller than that found during adsorption for all of the layers studied. This observation is in agreement with the general view that the electrostatic self-assembly method leads to essentially irreversible adsorption of the oppositely charged polyelectrolyte layers.

The upper panel of Figure 4b shows the time dependence of the so-called reduced frequency (the frequency, f, over the overtone number, ν). For purely elastic films (where the Sauerbrey equation is valid),[21,26] the results of $\Delta f/\nu$ corresponding to all overtones should collapse onto a single master curve. However, as seen from Figure 4b, they did not, indicating that, for the PDADMAC+PSS film, the rheological behavior is viscoelastic. This observation is further confirmed in the lower panel of Figure 4b by the behavior of the dissipation factor, D, that, after a short induction period, increases strongly during the adsorption process. D relates the dissipated and stored energies during the oscillation of the quartz sensor

$$D = \frac{E_{\text{dissipated}}}{2\pi E_{\text{stored}}} \tag{4}$$

where E_{stored} is the energy stored in the oscillating system and $E_{\text{dissipated}}$ is the energy dissipated during one period of oscillation.

A first consequence of the results in Figure 4 is that Sauerbrey's relation in eq 2 is not valid for calculating the actual adsorbed mass. A fit of the full experimental impedance spectra to the theoretical predictions has to be carried out.[21,26] Spectra corresponding to $\nu = 3$, 5, 7, 9, and 11 have been measured, thus making it possible to calculate the adsorbed mass, and the real and imaginary components of the complex shear modulus, $\hat{G}$, of the polymer layer ($\hat{G}$ was assumed frequency independent in the 15−55 MHz range)[34] defined as

$$\hat{\mathrm{G}} = \frac{1}{\hat{\mathrm{J}}} = G' + iG'' \tag{5}$$

where $\hat{J}$ is the complex shear compliance, and G' and G'' are the real and imaginary parts of the complex shear modulus, respectively, or in other words the elastic shear modulus and the viscous shear modulus.

Figure 5 shows adsorption dynamics for each polyelectrolyte determined by QCM at the solid/aqueous interface and expressed as mass adsorbed per unit of surface area, Γ, normalized by the infinite time adsorbed mass, Γ_∞. A clear difference is seen compared to the dynamic-tension results at the air/water interface in Figure 1. When expressed in normalized values, the LbL adsorption kinetics at the solid/

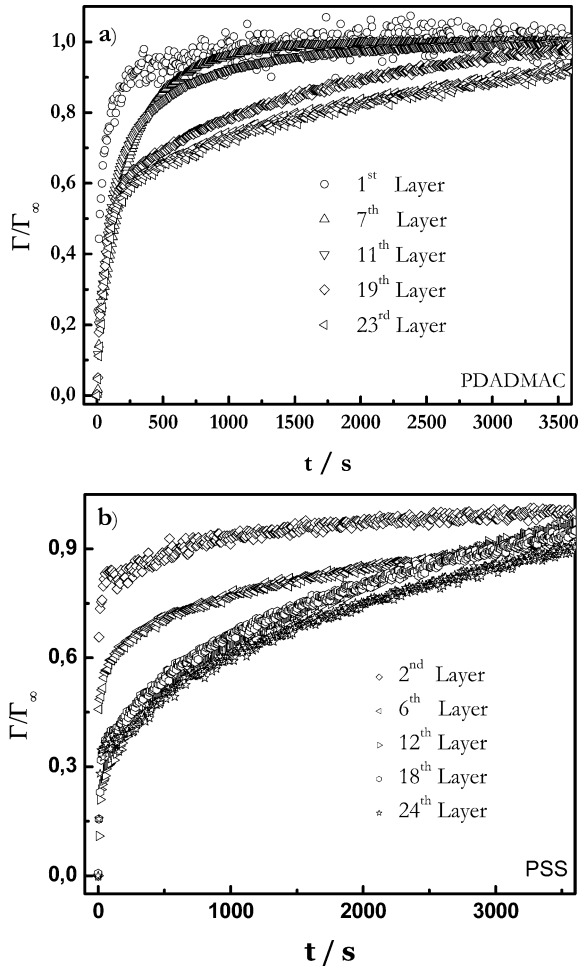

Figure 5. Normalized adsorption kinetics for (a) PDADMAC (top) and (b) PSS (bottom), at [NaCl] = 300 mM on the quartz sensor. $\Gamma = 0$ for all of the experiments corresponds to the adsorbed amount after the washout process of the previous layer.

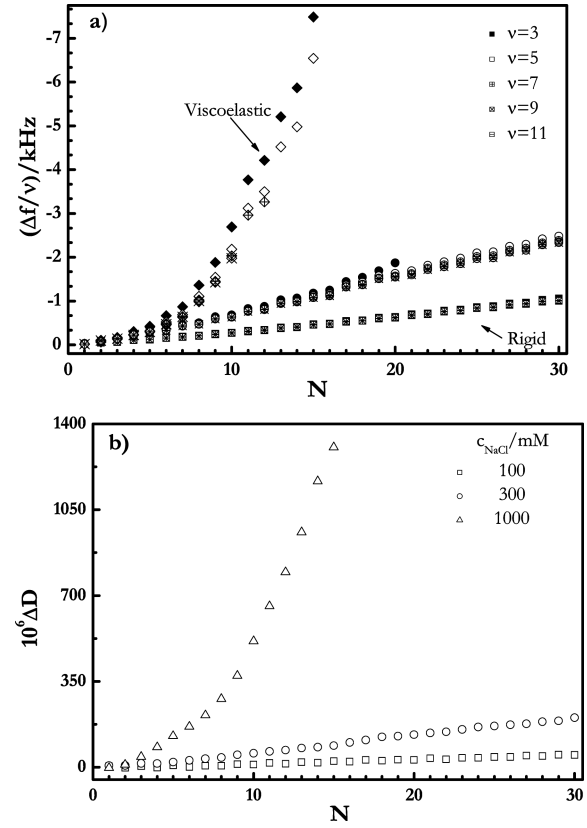

Figure 6. (a) Layer number dependence of the reduced frequency of the quartz crystal for the different overtones measured (overtones ν = 3, 5, 7, 9, and 11 are represented). At different ionic strengths, the symbols that represents the different salt concentrations are [NaCl] = 100 mM (squares), [NaCl] = 300 mM (circles), and [NaCl] = 1000 mM (diamonds). Notice that for low salt concentration the data of the different overtones collapse in a single curve (rigid film), whereas at high salt concentration the data of the different overtones lie on different curves (viscoelastic film); the different overtones are represented with different filled symbols. (b) Layer number dependence of the dissipation factor for the third overtone of the quartz crystal for different ionic strengths.

water interface slows as the layer number increases for both polyelectrolytes.

Parts a and b of Figure 6 summarize the changes in reduced frequency, $\Delta f/\nu$, and in dissipation factor, D, respectively, as the LbL multilayer grows. Increased ionic strength dramatically increases the frequency change (and the layer thickness). Also, at low salt concentrations, $\Delta f/\nu$ for the different overtones collapse onto a single master curve, indicating a rigid film.[24] The data scatter corresponding to high ionic strengths was due to different overtones following different $\Delta f/\nu$ versus N curves, thus indicating that the layers have viscoelastic character.

The dissipation factor was higher at high ionic strengths, in qualitative accordance with the dispersion found for the reduced frequency (Figure 6a), and also with the higher LbL thickness found by ellipsometry (Figure 3).

Discussion

Adsorption Kinetics. By graphing $\ln(\Gamma_\infty - \Gamma)$ versus t (or $\ln(\gamma_0 - \gamma)$ versus t), double-exponential kinetic behavior was clearly evident for both polyelectrolytes (Figures 7b and 8b), independent of the layer number. Therefore, following Raposo et al.,[35] we modeled the kinetics according to

$$\Gamma = A\left[1 - \exp\left(-\frac{t}{\tau_1}\right)\right] + B\left[1 - \exp\left(-\frac{t}{\tau_2}\right)\right]^m \qquad (6)$$

where Γ represents either the adsorbed mass density in the QCM or in the ellipsometric experiments, or $\gamma_0 - \gamma$ in the bubble experiments (γ_0 and γ are the surface tensions at the starting point of the adsorption process and in each moment, respectively). The exponent m was found to be unity for all experiments performed in this work. Thus, by setting $m = 1$ and by introducing the surface concentration in the limit of equilibrium as $\Gamma_\infty = A + B$, eq 6 is rewritten as

$$\Gamma = \Gamma_\infty - \mathrm{A}\exp\left(-\frac{t}{\tau_1}\right) - \mathrm{B}\exp\left(-\frac{t}{\tau_2}\right) \qquad (7)$$

where Γ_∞ is the equilibrium value for either the adsorption or tension change. The second term of eq 7 accounts for reorganization of the polymer chain after initial adsorption at the interface, according to Avrami's model for polymer crystallization.[36–38] Table 1 summarizes the best-fit values of the amplitudes A and B, and of the relaxation times τ_1 and τ_2 of eq 7 for the different layers at the air/water interface. In the case of the QCM experiments, the values of the adsorbed mass density Γ were calculated from the fit to the full impedance spectra.[21,26] All fitting was performed in a semilogarithmic scale to capture accurately the two distinct time constants.

Figures 7 and 8 show typical examples of the adsorption dynamics at the solid/water interface and the tension dynamics at the air/water interface, respectively. The dark lines in

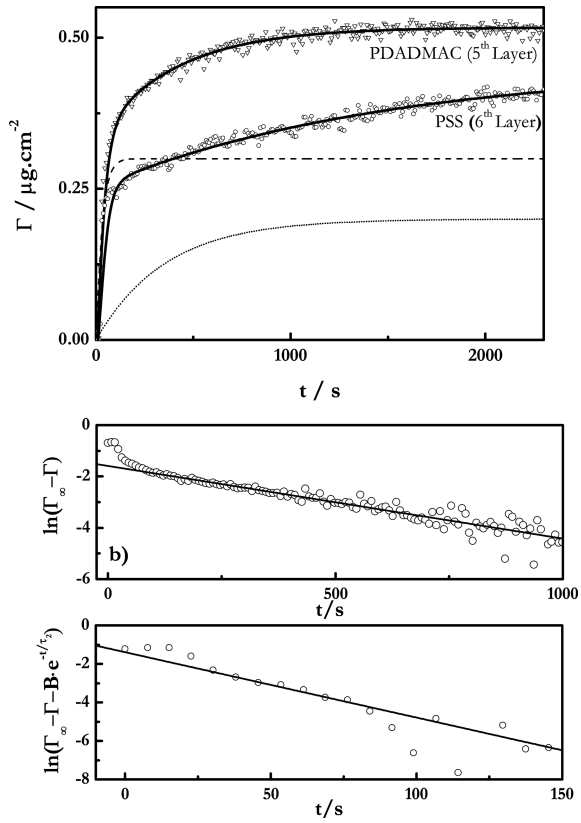

Figure 7. (a) Adsorption dynamics for layers of polyelectrolyte adsorbed in the multilayer PDADMA/PSS film over the quartz crystal. [NaCl] = 100 mM. Dark lines give the best fit to eq 7, for the PDADMAC layer with the parameters $A = 0.3 \pm 0.1$ $\mu g \cdot cm^{-2}$, $B = 0.20 \pm 0.01$ $\mu g \cdot cm^{-2}$, $\tau_1 = 29 \pm 7$ s, and $\tau_2 = 353 \pm 23$ s. For the PDADMAC layer, the two exponential components are shown: dashed line (fast kinetics); dotted line (slow kinetics). (b) Logarithmic analysis of the adsorption dynamics for the PDADMAC layer shown in part a.

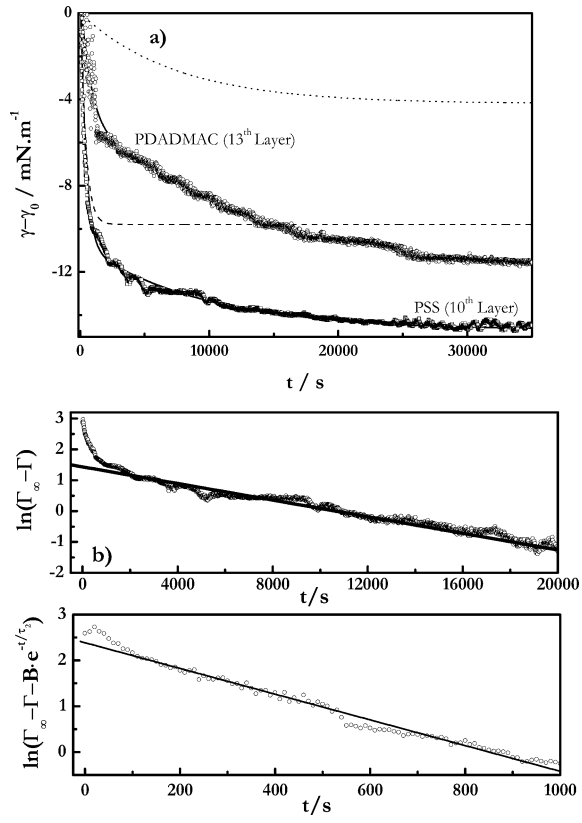

Figure 8. (a) Tension dynamics for layers of polyelectrolyte adsorbed in the multilayer PDADMAC/PSS film at the air/water interface. $I =$ 150 mM. Dark lines give the best fit to eq 7, for the PSS layer with the parameters $A = 9.8 \pm 0.3$ $mN \cdot m^{-1}$, $B = 4.20 \pm 0.03$ $mN \cdot m^{-1}$, $\tau_1 = 400 \pm 20$ s, and $\tau_2 = 7400 \pm 100$ s. For the PSS layer, the two exponential components are also shown: dashed line (fast kinetics); dotted line (slow kinetics). (b) Logarithmic analysis of the tension dynamics for the PSS layer shown in part a.

part a of these figures represent the best fits to eq 7. Table 1 lists the resulting characteristic adsorption time and the corresponding amplitudes for the air/water interface; Figure 9 shows these same parameters as a function of layer number for the solid/water interface. The dotted and dashed lines in Figures 7a and 8a illustrate the individual contributions of the two exponential processes: PDADMAC at the solid/water interface and PSS at the air/water interface. When the fast kinetic process asymptotes, most of the mass has already adsorbed (75−80% in most cases) and, likewise, most of the tension change has been accomplished. Figures 7b and 8b illustrate the long and short time behavior for the adsorption process at both studied interfaces.

In general, the kinetics of surface-tension change at the air/water interface was slower than the adsorption kinetics at the solid/water interface. We note that $\gamma(t)$ does not directly reflect adsorption kinetics at the air/water interface. For example, surface tension can continue to fall with little change in adsorbed mass due to slow molecular rearrangement. Nevertheless, both the $\gamma(t)$ curves at the air/water interface and the $\Gamma(t)$ curves at the solid/water interface consist of two distinct time processes. The first contribution corresponds to the diffusion/initial adsorption of the polymer from the aqueous solution, and the second to the reorganization of the preadsorbed polymer. These two contributions lead to the total surface coverage of each layer. The slow rearrangement process was especially evident for adsorption of PDADMAC at the air/water interface with $N > 7$ in Table 1. Initially, the bubble/aqueous interface has a rather small negative charge that is reduced further by the high ionic strength, Thus, only a small amount of cationic PDADMAC adsorbs. As a consequence, adsorption of subsequent layers simply reflects smaller surface-charge densities. Figure 9a demonstrates that the slow rearrangement time constant for each layer at the solid/water interface increases with N (notice the log scale of the abscissa in Figure 9). However, the fast kinetic process was only slightly affected by the layer number for PDADMAC and not at all for PSS. Conversely, the kinetics of multilayers built at the air/water interface for $N > 7$ were only affected by the nature of the polyelectrolyte adsorbed in the previous layer, and not by the number of layers.

Water Content. Before comparing the mechanical properties of the solid-supported and liquid-supported films, it is necessary that the water contents of the films are the same. Appendix A describes how the film water content was calculated from QCM and ellipsometry measurements. Figure 10 shows the mass fraction of water, X_w, for the films studied. For similar aqueous ionic strengths, the water content of solid-supported and liquid-supported films is the same within the experimental uncertainty. Also, it is clear that water content decreases as N increases, and that, for a given value of N, water content increases with increasing ionic strength. We conclude that the polyelectrolyte LBL films studied in this work are highly plasticized by water. Therefore, the film glassy state is well below room temperature. Further, the

TABLE 1: Parameters of the Double-Exponential Sorption Kinetics Processes in eq 7, for the Air/Water Interface

polymer	N	A/mN·m^{-1}	$10^{-1}\cdot\tau_1$/s	B/mN·m^{-1}	$10^{-2}\cdot\tau_2$/s
PDADMAC	$N \leq 6$	4.1 ± 0.6	11 ± 2	2.1 ± 0.2	10 ± 2
	$N \geq 7$	5.3 ± 0.1	10 ± 2	7.45 ± 0.02	141 ± 1
PSS	$N = 1$	2 ± 1	23 ± 9	0.5 ± 0.2	11 ± 5
	$N \geq 2$	9.8 ± 0.3	40 ± 2	4.20 ± 0.03	74 ± 1

water content of the LbL multilayers studied here is independent of the interface at which they are built.

Mechanical Properties. Ferri et al.[15] have discussed the calculation of the surface Young's modulus E_Y of the polymer layer adsorbed at the air/water interface from the dilational modulus of the adsorbed layer E_s

$$E_s = \frac{E_Y}{2(1-\nu_s)} \tag{8}$$

where ν_s is the Poisson ratio of the layer. Following Ferri et al.[17] and Monroy et al.,[39] we have used $\nu_s = -1$ in this work. However, adoption of $\nu_s = 0$ does not change qualitatively the conclusions of this work. Values of E_s have been calculated at the air/water interface from the usual formula

$$E_s(t) = A(t)\left(\frac{\partial\gamma(t)}{\partial A(t)}\right)_T \tag{9}$$

where $A(t)$ is the area of the air bubble immersed in the polymer solution. In our step-strain experiments, A was kept constant after the expansion, and $\gamma(t)$ was fit to eq 9. Table 2 collects the values of $E_{s,0}$ [$\equiv E_s(t = 0)$] and $E_{s,\infty}$ [$\equiv E_s(t = \infty)$] for the different adsorbed layers at the air/water interface. The results show variation with N. As expected for a hydrated polymer layer, the values of the modulus corresponded to a gel-like material. This result is slightly different from that of Sefouane et al.[18] for a PSS/poly(allylamine) LbL film who reported values of E_s (at 200 Hz) that were small and independent of N (for $N \leq 4$) and then increased sharply for thicker multilayers.

The bulk elastic modulus of the film can be calculated by normalizing the surface modulus by the film thickness, i.e., $E = E_s/h_{op}$, with h_{op} obtained from the ellipsometric results (Figure 3).[17,40] Gardner et al.[41] indicate that for insoluble monolayers the interfacial stress upon a dilational deformation is comprised of both a static value and a dynamic contribution, which has been verified experimentally.[42,43] The two components of the dilational deformation were obtained after normalizing with the thickness of the values of $E_{s,0}$ [$\equiv E_s(t = 0)$] for the static contribution and $E_{s,\infty}$ [$\equiv E_s(t = \infty)$] for the dynamic one (see above). To separate the dynamic contribution to E' at a given frequency from the static contribution, E_∞, Freer et al.[44] introduced a recoverable dilational storage modulus $\delta E = E' - E_\infty$, and found a very good correlation between δE and G' for protein monolayers. The values of δE are also plotted in Figure 11 together with the values of G' for the multilayers at the solid/water obtained from the analysis of the QCM data, and both increase almost linearly with N. Within experimental scatter, the values of δE and of G' agree when compared at similar ionic strengths. Freer et al. found that $\delta E > G'$ for lysozyme and the β-casein monolayers at the hexadecane/water interface.[44] As it can be observed in Figure 11, higher ionic strengths lead to an increase in G' for a given value of N. This result is in accord with the increase of the adsorbed-layer thickness upon increasing the ionic strength (Figure 3). This ionic-strength effect has previously been reported for polymer monolayers adsorbed on the solid/water interface.[45]

The δE and G' values shown in Figure 11 are typical of polymers in the rubbery state, and in aqueous gels. Mueller et al.[3] have studied microcapsules made of PDADMAC/PSS multilayers with eight layers. The mechanical properties of their LbL films were measured by AFM. They concluded that the

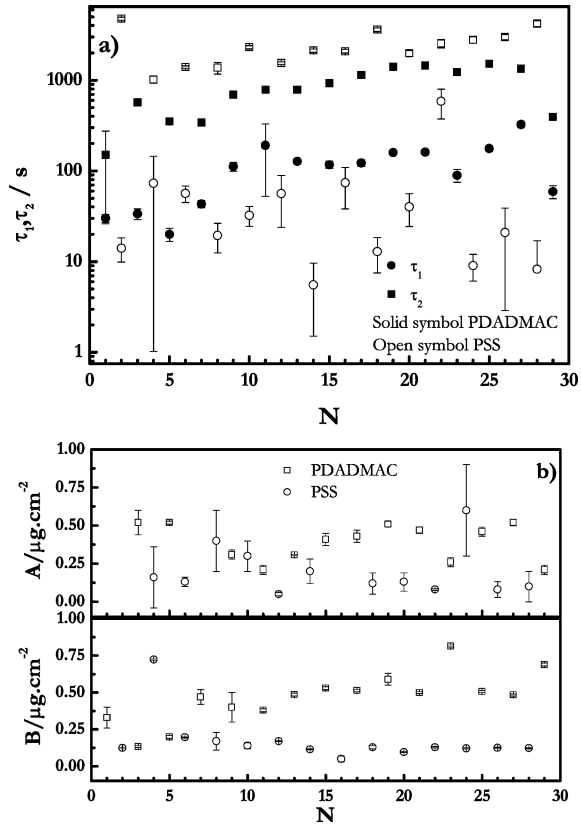

Figure 9. (a) Layer number dependence of the adsorption time constants of the PDADMAC/PSS multilayer on a quartz crystal at [NaCl] = 100 mM. Solid symbols correspond to PDADMAC, and open symbols correspond to PSS. Circles reflect the fast adsorption process, and squares represent the slow rearrangement process. (b) Layer number dependence of the amplitude of the two kinetic steps for the experiment show in part a.

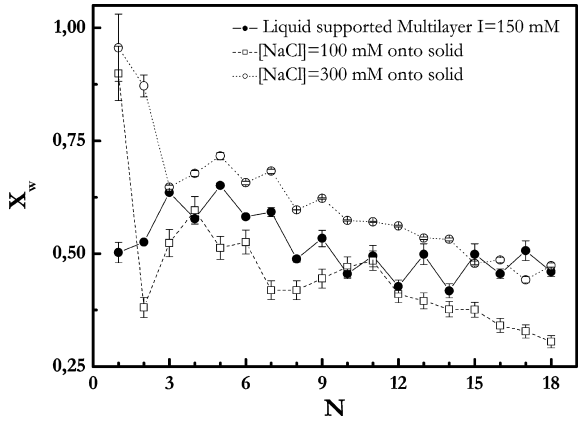

Figure 10. Layer number of dependence of the multilayer water mass fraction, X_w.

TABLE 2: Values of $E_{s,0}$ and $E_{s,\infty}$ for the Different Adsorbed Layers at the Air/Water Interface

PDADMAC	N	1	3	5	7	9	11	13
	$E_{s,0}$/mN·m^{-1}	0	0	426	265	380	367	214
	$E_{s,\infty}$/mN·m^{-1}	0	0	18	132	93	4	69
PSS	N	2	4	6	10	12		
	$E_{s,0}$/mN·m^{-1}	131	131	3	206	383		
	$E_{s,\infty}$/mN·m^{-1}	108	65	3	116	329		

elasticity modulus was of the order of GPa, i.e., 3 orders of magnitude larger than the present data. However, for nanocapsules of poly(allylamine)/PSS (PAH/PSS), the values obtained were in the range of MPa.[4] Heuvingh et al.[4] concluded that the films of PDADMAC/PSS were in a glassy state, whereas those of PAH/PSS were in a rubbery state. Surprisingly, Mueller et al.[3] and Heuvingh et al.[4] stress that the elasticity modulus of Salomäki et al.[46] for flat films of PDADMAC/PSS is much smaller (a few MPa), in agreement with the results of the present work. Therefore, the morphology of the multilayers has a strong effect on their mechanical properties.

Charge Compensation. The surface charge built upon adsorption of a polyelectrolyte must be neutralized by monomers of the preceding polymer layer (intrinsic mechanism), or by counterions (extrinsic mechanism),[47] as sketched in Figure 12. It has been shown for sequential bilayers that the charge-compensation mechanism has important effects on the thickness of the multilayer film.[23,48,49] For both PSS/poly(allylamine)[48] and poly(*N*-methyl-2-vinyl pyridinium chloride)/PSS[49] films, the intrinsic neutralization mechanism leads to a linear dependence of the thickness on the number of layers, i.e., the thickness of each bilayer is nearly constant. This behavior is found here in the films grown at the air/aqueous solution interface and at the solid/water interface when grown at the lowest ionic strength. The extrinsic neutralization mechanism usually leads to layers

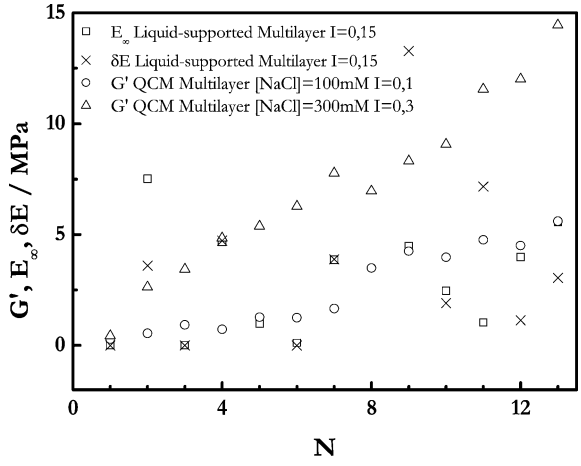

Figure 11. Layer number dependence of the mechanical properties of the LbL films. The first layer was PDADMAC. $E_{s,\infty}$ is the real part of the surface Young's modulus for $t = \infty$ calculated from the step-expansion experiments of the air/water interface. $\delta E = E' - E_\infty$. The real part of the shear modulus, G', is calculated from the QCM experiments on the multilayers at the solid/water interface.

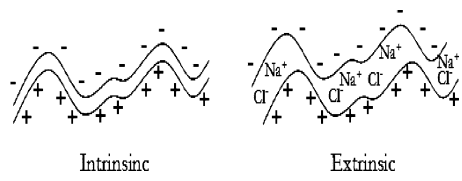

Figure 12. Schematic of the intrinsic- versus extrinsic-charge-compensation mechanisms in electrostatic LbL self-assembly.

TABLE 3: Ratio of the Number of Monomers of PDADMAC to Those of PSS, $\Gamma_m(1)/\Gamma_m(2)$, Adsorbed in Each Bilayer per Unit Area

			$\Gamma_m(1)/\Gamma_m(2)$
air/water interface	PDAMAC:PSSNa		1
solid/water interface	[NaCl] = 100 M	$N \leq 16$	1
		$N > 16$	3.7
	[NaCl] = 300 M	$N \leq 12$	1
		$N > 12$	6.5

whose thicknesses increase with N faster than linearly. This is frequently referred to as exponential growth,[24] even though it may not be always rigorously so. In the exponential-growth case, the thickness of each layer increases with N. This is the case found here for the solid-supported films grown at high ionic strength (see Figure 3).

A simple way to corroborate the correlation between the charge-compensation mechanism and the thickness-growth behavior is to investigate whether the number of PDADMAC monomers adsorbed per PSS monomer adsorbed changes as the ionic strength changes. In the ideal case, the ratio of monomers of PDADMAC, $\Gamma_m(1)$, and of PSS, $\Gamma_m(2)$, should change from unity for perfect intrinsic compensation to a value larger or smaller than unity for extrinsic compensation. Values of $\Gamma_m(1)/\Gamma_m(2) \approx 1$ should correspond to the linear-growth regime. The ellipsometric measurements allowed us to calculate the mass adsorbed in each adsorbed layer (see Appendix B). Calculation of the number of monomers of PDADMAC and of PSS adsorbed follows directly The ratio $\Gamma_m(1)/\Gamma_m(2)$ is shown in Table 3. $\Gamma_m(1)/\Gamma_m(2) = 1$ for the air/water interface, thus supporting the intrinsic-charge-compensation mechanism. However, this ratio was higher for the solid/water interface, and the values of $\Gamma_m(1)/\Gamma_m(2)$ increased with the ionic strength. A possible explanation is that once a PSS layer adsorbs, only part of the PDADMAC subunits of the next layer adsorb directly onto the PSS ones. Some parts of the PDADMAC chains form loops and/or tails dangling into the aqueous phase. These dangling units are charge compensated by solution counterions. In the case of the extrinsic-charge-compensation mechanism, Picart et al.[50] proposed that one of the polyelectrolytes diffused "in" and "out" of the multilayer during the adsorption process.[50] This process might also strongly affect the adsorption kinetics, especially the slow process that we have attributed to reorganization of the preadsorbed polymers. The effect of possible PDADMAC interlayer diffusion is clearly more important for small values of N, whereas, for thick enough multilayers, the densification of the intermediate layers (zone II)[15] slows diffusion. Thus, the observed kinetics become dominated by the outer layers (zone III). Interlayer diffusion does not take place for thick layers. As a consequence, only for the first layers (where the interaction of the polymer with the initial substrate is relevant) might differences be expected between solid-supported and liquid-supported films.

The two different types of charge compensation found for the air/water and solid/water interfaces also imply differences in the physics of the adsorption process. The intrinsic mechanism

implies a Coulombic interaction between monomers of PDADMAC and of PSS. Adsorption is accompanied by a large increase of entropy associated with the release of counterions into the bulk of the solution. Such a large entropic increase is not expected for the extrinsic-charge-compensation adsorption mechanism and the corresponding nonlinear growth of the multilayer thickness. However, in extrinsic-charge compensation the possible existence of polymer loops and tails makes the entropy decrease associated with the lost of conformations upon adsorption smaller than typical for the adsorption of a polymer chain. It must be stressed that the correlation found in this paper between the charge-compensation mechanism and the thickness-growth behavior has been tested experimentally only for the electrostatic PDADMAC/PSS LbL films studied here, and for two other multilayers.[47,48] Therefore, more systems should be studied before it can be considered as general for electrostatic self-assembled multilayers.

Conclusions

The kinetics of adsorption of anionic PSS and cationic PDADMAC at the air/water and solid/water interfaces has been measured as a function of the number of layers during LbL growth of PSS/PDADMAC multilayers. Adsorption of both polymers at both interfaces follows double-exponential-growth kinetics with two time constants corresponding to a fast diffusion/initial adsorption process followed by a slow configuration change. At the air/water interface, the adsorption kinetics of PSS does not depend on the number of layers except for the first. This behavior contrasts with that found at the solid/water interface where the fast mode is not affected by the number of layers of the film and the slow mode slows as the number of layer increases. Similar results were found for the adsorption of PDADMAC except that for the air/water interface two clearly different kinetics were found for films with less and with more than seven layers of PDADMAC.

The recoverable dilational storage modulus δE of the liquid-supported films was measured by the step-expansion-relaxation experiments on a bubble tensiometer. For a given film, the values of δE agree with the real component of the shear modulus G' measured at the solid/water interface by a dissipative quartz crystal microbalance. Both δE and G' increase slightly with increasing number of layers of the multilayers. The values of G' are in the 1−5 MPa, typical of swelled polymer gels.

The ellipsometry results indicate that at the air/water interface the multilayer grows by an intrinsic-charge-compensation mechanism, whereas, at the solid/water interface, the mechanism switches from an intrinsic mechanism (for less than approximately 12 layers) to an extrinsic-charge-compensation mechanism for thicker layers. Linear growth of the LbL film thickness is expected for the intrinsic mechanism, whereas nonlinear growth is usually found for the extrinsic one.

Appendix A: Multilayer Water Content

Following the method described by Halthur et al.,[51] it is possible to estimate the water content of the solid-supported multilayer by comparing the masses obtained by QCM and by ellipsometry. In all of the solid-supported multilayers studied, we found that the acoustical thickness is larger than the optical one. This is due to the fact that ellipsometry is almost insensitive to the adsorbed solvent because its refractive index is close to that of the solvent layer above the multilayer. As a consequence, the water mass fraction, X_w, can be estimated using the following expression[21,29,51]

$$X_w = \frac{h_{ac} - h_{op}}{h_{op}} \tag{A.1}$$

where h_{ac} and h_{op} are the acoustical (QCM) and optical thickness (ellipsometry), respectively. We found that the values obtained for this approximation are in good agreement with the ones found by neutron reflectivity experiments.[52]

An alternative method for the calculation of the water content is based solely on the ellipsometric results[53] using the following pair of expressions

$$\left(\frac{dn}{dc}\right)_T = \frac{(n_p - n_s)}{\rho_p} \tag{A.2}$$

and

$$n_f = X_w n_p + (1 - X_w) n_s \tag{A.3}$$

where $(dn/dc)_T$ is the isothermal differential index of refraction [the values of $(dn/dc)_T$ obtained for PDADMAC and PSS at 25 °C were 0.213 and 0.178 cm^3/g, respectively], ρ_p is the density of the polymer (1.2 ± 0.1 $g \cdot cm^{-3}$),[24] n_p is the refractive index for the polymer, n_s is the refractive index of the solvent (in our case the aqueous solution), and n_f is the refractive index of the multilayer obtained from the analysis of the ellipsometric results (data not shown). This method was used to calculate the water content for the liquid-supported multilayer. Application of this alternative method for solid-supported multilayers with 18 layers was in good agreement with the previous method: X_w ([NaCl] = 100 mM) = 0.2 ± 0.1 and X_w ([NaCl] = 100 mM) = 0.3 ± 0.1. A similar approach has been used for polypeptide multilayers.[51] The values of X_w for the systems studied in this work are shown in Figure 10.

Appendix B: Multilayer Monomer Density

By combining the results obtained from ellipsometry and the $(dn/dc)_T$ measurements, it is possible to estimate the monomer layer density, Γ_m, in each layer and, as a consequence, to analyze the charge-compensation mechanism in consecutive layers. The monomer layer density is related to the adsorbed mass, Γ, by

$$\Gamma_m = \frac{N_{Av}\Gamma}{M_w} \tag{B.1}$$

where M_w is the molecular weight of the monomer and N_{Av} is Avogadro's number. Γ is obtained using De Feijter's equation[54]

$$\Gamma = \frac{(n_f - n_s)h_{op}}{(dn/dc)_T} \tag{B.2}$$

where the symbols are the same as those in eqs A.1 and A.2.

Upon combining eqs B.1 and B.2, we calculated Γ_m for all of the consecutive layers. Let $\Gamma_m(1)$ and $\Gamma_m(2)$ denote the monomer surface density of two consecutive layers (polycation and polyanion, respectively). When $\Gamma_m(1)/\Gamma_m(2) \sim 1$, it can be assumed that the charge compensation is intrinsic, whereas, when $\Gamma_m(1)/\Gamma_m(2) \neq 1$, it can be assumed that the mechanism of charge compensation must be considered as extrinsic.

Acknowledgment. The work done in Madrid was supported in part by MICINN under grants FIS2006-12281-C02-01 and CTQ2006-6208/BQU and by CAM under grant INTERFASES S05-MAT-227. E.G. was supported by an FPU fellowship from MICINN, and H.R. was supported by a Juan de la Cierva contract from MICINN. The authors are grateful to the UIRC of the Universidad Complutense de Madrid, in particular to J. E. F. Rubio for helping us with the ellipsometric measurements.

References and Notes

(1) Jones, R. A. L. *Soft Machines: Nanotechnology and Life*; Oxford University Press: Oxford, U.K., 2004.

(2) Garbassi, F.; Morra, M.; Occhiello, E. *Polymer Surfaces: From Physics to Technology*; John Wiley & Sons: Chichester, U.K., 1998.

(3) Mueller, R.; Khler, K.; Shukorukov, G.; Fery, A. *Macromolecules* **2005**, *38*, 9766.

(4) Heuvingh, J.; Zappa, M.; Fery, A. *Langmuir* **2005**, *21*, 3165.

(5) Dong, W.-F.; Ferri, J. K.; Adalsteinsson, T.; Schönhoff, M.; Sukhorukov, G. B.; Möhwald, H. *Chem. Mater.* **2005**, *17*, 2603.

(6) Beneventi, D.; Pugh, R. J.; Carré, B.; Gandini, A. *J. Colloid Interface Sci.* **2003**, *268*, 221.

(7) Klein, J.; Kumacheva, E. *Science* **1995**, *269*, 816.

(8) Keddy, J. L.; Jones, R. A. L.; Cory, R. A. *Europhys. Lett.* **1994**, *27*, 59.

(9) Forrest, J. A.; Mattsson, J. *Phys. Rev.* **2000**, *61*, R53.

(10) Sergei, A.; Huth, H.; Schick, C.; Kremer, F. *Macromolecules* **2008**, *41*, 3636.

(11) Riande, E.; Díaz-Calleja, R.; Prolongo, M. G.; Masegosa, R. M.; Salom, C. *Polymer Viscoelasticity: Stress and Strain in Practice*; Marcel Dekker: New York, 2000.

(12) Jiang, C.; Markutsya, S.; Tsukruk, V. V. *Adv. Mater.* **2004**, *16*, 157.

(13) Hilles, H. M.; Ortega, F.; Rubio, R. G.; Monroy, F. *Phys. Rev. Lett.* **2004**, *92*, 255503.

(14) Ulmann, A. *Ultrathin Organic Films: From Langmuir-Blodgett to Self-Assembly*; Academic Press: San Diego, CA, 1991.

(15) Decher, G.; Schlenoff, J. F. *Multilayer Thin Films*; Wiley-VCH: Weinheim, Germany, 2003.

(16) Ferri, J. K.; Dong, W.-F.; Miller, R. *J. Phys. Chem. B* **2005**, *109*, 14764.

(17) Ferri, J. K.; Dong, W.-F.; Miller, R.; Möhwald, H. *Macromolecules* **2006**, *39*, 1532.

(18) Safouane, M.; Miller, R.; Möhwald, H. *J. Colloid Interface Sci.* **2005**, *292*, 86.

(19) Fretigny, C.; Basire, C. *J. Appl. Phys.* **1997**, *82*, 43.

(20) Dai, X.; Zhang, Y.; Guan, Y.; Yang, S.; Xu, J. *Thin Solid Films* **2005**, *474*, 159.

(21) Janshoff, A.; Galla, H.-J.; Steinem, C. *Angew. Chem., Int. Ed.* **2000**, *39*, 4004. Höök, F.; Kasemo, B.; Nylander, T.; Fant, C.; Sott, K.; Elwing, H. *Anal. Chem.* **2001**, *73*, 5796.

(22) Olanya, G.; Iruthayaraj, J.; Poptoshev, E.; Makuska, R.; Vareikis, A.; Claesson, P. M. *Langmuir* **2008**, *24*, 5341.

(23) Schlenoff, J. B.; Dubas, S. T. *Macromolecules* **2001**, *34*, 592.

(24) Dubas, S. T.; Schlenoff, J. B. *Macromolecules* **1999**, *32*, 8153.

(25) Love, J. C.; Estroff, L. A.; Kriebel, J. K.; Nuzzo, R. G.; Whitesides, G. M. *Chem. Rev.* **2005**, *105*, 1103.

(26) Johannsmann, D.; Mathauer, K.; Wegner, G.; Knoll, W. *Phys. Rev. B* **1992**, *46*, 7808.

(27) Azzam, R. M. A., Bashara, N. M. *Ellipsometry and polarized light*; Elsevier: North-Holland, 1987.

(28) Craig, V. S. J.; Plunkett, M. *J. Colloid Interface Sci.* **2003**, *262*, 126. Benjamins, J.-W.; Thuresson, K.; Nylander, T. *Langmuir* **2005**, *21*, 149.

(29) Vörös, J. *Biophys. J.* **2004**, *87*, 553.

(30) Svitova, T.; Radke, C. J. *Ind. Eng. Chem. Res.* **2005**, *44*, 1129. Svitova, T. F.; Wetherbee, M. J.; Radke, C. J. *J. Colloid Interface Sci.* **2003**, *261*, 170.

(31) Neumann, A. W.; Spelt, J. K. *Applied Surface Thermodynamics*; Marcel Dekker: New York, 1996.

(32) Klebanau, A.; Kliabanova, N.; Ortega, F.; Monroy, F.; Rubio, R. G.; Starov, V. *J. Phys. Chem. B* **2005**, *109*, 18316.

(33) Tompkins, H. G. *A User's Guide to Ellipsometry*; Academic Press Inc.: London, 1993.

(34) Steinem C.; Janshoff, A. *Piezoelectric Sensors*; Springer-Verlag: Berlin, 2007.

(35) Raposo, M.; Pontes, R. S.; Mattoso, L. H. C.; Oliveira, O. N. *Macromolecules* **1997**, *30*, 6095.

(36) Strobl, G. *The Physics of Polymers*, 2ns ed.; Springer: Berlin, 1997.

(37) Chiang, C.-Y.; Starov, V. M.; Lloyd, D. R. *Colloid J. (Russian Academy of Sciences, English Translation)* **1995**, *57*, 715.

(38) Chiang, C.-Y.; Starov, V. M.; Hall, M. S.; Lloyd, D. R. *Colloid J. (Russian Academy of Sciences, English Translation)* **1997**, *59*, 715.

(39) Monroy, F.; Ortega, F.; Rubio, R. G. *Eur. Phys. J. B* **2000**, *13*, 745.

(40) Dimova, R.; Danov, K.; Pouligny, B.; Ivanov, I. *J. Colloid Interface Sci.* **2000**, *226*, 35.

(41) Gardner, J. W.; Addison, J. V.; Schechter, R. S. *AIChE J.* **1978**, *24*, 400.

(42) Saulnier, P.; Boury, F.; Malzert, A.; Heurtault, B.; Ivanova, T.; Cagna, A.; Panaiotov, I.; Proust, J. E. *Langmuir* **2001**, *17*, 8104.

(43) Monroy, F.; Rivillon, S.; Ortega, F.; Rubio, R. G. *J. Chem. Phys.* **2001**, *115*, 530.

(44) Freer, E. M.; Yim, K. S.; Fuller, G. G.; Radke, C. J. *J. Phys. Chem.* **2004**, *108*, 3835.

(45) Naderi, A.; Iruthayaraj, J.; Pettersson, T.; Makuska, R.; Claesson, P. M. *Langmuir* **2008**, *24*, 6676.

(46) Salomäki, M.; Laiho, T.; Kankare, J. *Langmuir* **2004**, *20*, 9585–9590.

(47) Jomaa, H. W.; Schlenoff, J. B. *Macromolecules* **2005**, *38*, 8473.

(48) Schlenoff, J. B.; Ly, H.; Li, M. *J. Am. Chem. Soc.* **1998**, *120*, 7626.

(49) Jaber, J. A.; Schlenoff, J. B. *Langmuir* **2007**, *23*, 896.

(50) Picart, C.; J. Mutterer, J.; Richert, L.; Luo, Y.; Prestwisch, G. D.; Schaff, P.; Voegel, J. C.; Lavalle, P. *Proc. Natl. Acad. Sci. U.S.A.* **2002**, *99*, 12531.

(51) Halthur, T. J.; Elofsson, U. *Langmuir* **2004**, *20*, 1739.

(52) Guzmán, E.; Ritacco, H.; Rubio, J. E. F.; Rubio, R. G.; Ortega, F. *Soft Matter*, in press.

(53) Ball, V.; Ramsden, J. J. *Biopolymers* **1998**, *46*, 489.

(54) De Feijter, J. A.; Benjamins, J.; Veer, F. A. *Biopolymers* **1978**, *17*, 1759.

JP811178A